Spectral unmixing for thermal infrared multi-spectral airborne imagery over urban environments: day and night synergy

Carlos Granero-Belinchon, Aurélie Michel, Véronique Achard, Xavier Briottet

MDPI

Article

Spectral unmixing for thermal infrared multi-spectral airborne imagery over urban environments: day and night synergy

Carlos Granero-Belinchon [1,*], Aurelie Michel [1], Veronique Achard [1] and Xavier Briottet [1]

[1] ONERA-DOTA, University of Toulouse, FR-31055 Toulouse, France; aurelie.michel@onera.fr (A.M.); veronique.achard@onera.fr (V.A.); xavier.briottet@onera.fr (X.B.)

Version April 28, 2020 submitted to Remote Sens.

Abstract: This article aims to show that TRUST thermal unmixing, providing intra-pixel information of material abundances and their temperatures, allows a better description of the urban thermography, which not only supplies land surface temperatures at better resolutions but also allows to link them to specific materials. Moreover, this article presents an improved version of TRUST, called TRUST-DNS (Day and Night Synergy), which takes advantage of daytime and nighttime acquisitions to improve the unmixing performances. Both TRUST and TRUST-DNS are applied on airborne thermal images of Madrid city center obtained during the DESIREX campaign 2008, initially at 4m resolution and undersampled to 8m resolution. This undersampling allows to use the 4m ground classification done during the DESIREX campaign as reference for the abundance retrieval study. Thus, this article aims at showing the applicability of TRUST thermal unmixing on a highly challenging study case: the analysis of a heterogeneous urban environment with airborne multispectral (8 thermal bands) images at 8m resolution. In this study, seven different endmembers (natural and manmade materials) are considered as composing the Madrid city center, and TRUST and TRUST-DNS are used to recover intra-pixel abundance and temperature maps at 8m resolution for each endmember.

Keywords: Thermal unmixing; TRUST; Urban environment; Airborne remote sensing; LST

1. Introduction

Global warming influences every region of the world. Its effects have been visible for a long time: ice loss in the poles with the consequent increase of the sea level, extreme meteorological conditions with an increase in rainfalls but also more frequent droughts, increase in the frequency and intensity of heat waves [1] *etc*. Europe is already suffering the impacts of climate change. Both the center and the south of the continent present heat waves, forest fires and droughts more frequently than in the past. Furthermore, the european urban regions, where 80% of europeans live, are exposed to extremely strong heat waves which appear more and more frequently [1].

Urban environments are suffering sharper increases of their temperatures compared to rural areas. This is known as Urban Heat Island (UHI) effect [2], which has been well documented for a large number of cities across the world [2]. Multiple agents causing UHI have been detected, such as: human activity, population growth, land cover modification and, of course, global warming [2]. Moreover, UHI has been identified as producing air pollution increase, population health issues and to alter the energy consumption needs. Heat waves in Europe are more and more frequent and intense. This summer (2019) the heat waves in France produced temperatures of 45^o C, 4.5^o C higher than the heat waves of 2003 which have

been estimated to kill around 70000 people in Europe [3]. Solutions to stop this increase of heat waves frequencies and intensities are required, and these must cover urban planning. In order of measures to be adapted to face the problem, a good understanding of the sources, causes and dynamics of urban warming is needed.

Usually, UHI makes reference to the air temperature difference between rural and urban areas[4]. However, air temperature data covering a large spatial area are unusual due to the location (in space) of the measures [5,6]. Airborne remote sensing, covering large areas usually including both urban and rural areas around, allows to study the Surface Urban Heat Island (SUHI) effect, defined as the Land Surface Temperature (LST) difference between rural and urban areas [7]. Although SUHI is dominated by different physics than UHI, they have been shown to be correlated, especially during night [7].

However, even if airborne remote sensing provides high spatial resolution images (some of meters), higher resolutions are sometimes needed to analyse the correlation between LST and urban materials, allowing to identify sources and wells of SUHI. For this kind of analysis looking at linking LST to a given material, and then to identify which kind of materials leads to the occurrence of SUHI, thermal unmixing methods can be extremely efficient [8–10]. This kind of methods provides abundance and temperature maps, for a given number of scene materials (previously defined) and from a given thermal radiance image. Then, they allow to understand how the different materials behave in function of their sun exposure, their location, or the moment of the day (if several images at different acquisition times are available) among other factors [8–10].

Initially, reflective-thermal approaches were developed [8]. These methodologies were based on two steps: 1) the estimation of intra-pixel material abundances by using radiances from the reflective domain together with classical reflective unmixing methods [8,11], and 2) the estimation of intra-pixel temperatures by using thermal radiances and these previously obtained intra-pixel abundances. However, the need of bands in the reflective domain avoids nighttime application, where SUHI and UHI are more correlated, but also where reflective radiances are not available. In addition, to perform future high-spatial resolution studies in cities, Unmanned Aerial Vehicles (UAVs) appear as ideal [12], and having only thermal bands can allow to reduce UAV mission costs.

Currently, different thermal unmixing approaches using only Thermal InfraRed (TIR) bands exist. Thus among the first developed methodologies, the Temperature and Emissivity Separation using Spectral Mixture Analysis (TESSMA) supposes homogeneous intra-pixel temperatures [13] and is hence not perfectly adapted to thermal unmixing [14]. On the other hand, classical spectral unmixing methods, such as Fully Constrained Linear Square Unmixing (FCLSU) [11], can be applied on the thermal domain by considering the couple of temperature and emissivity spectra to define a given material [15]. However, this approach considers the temperature of a given material to be constant across the image. Emissivity based unmixing method grounds on the application of classical spectral linear unmixing methods on the emissivity spectra to obtain the intra-pixel abundances to next estimate the intra-pixel temperatures by considering the black body law of a composed flat surface [9]. The main issue of this method is that it does not consider material temperature differences when estimating the abundances, and then it looses a principal source of TIR information during unmixing. Finally, among the most advanced methods, Thermal Remote sensing Unmixing for Subpixel Temperature (TRUST) allows to jointly estimate the intra-pixel abundances and temperatures by minimizing the radiance reconstructed error [10]. This method also allows intra-pixel temperature variations and variations in the material temperatures across the image. The best performances of TRUST over other thermal unmixing methods have been already shown for simple scenarios such as roofs composed of three materials, for high spatial resolutions of about 1m, and for hyperspectral imagery with more than 30 thermal bands [10,15].

This article aims at illustrating the applicability of TRUST on highly heterogenous urban environment multispectral (8 bands) images at 8m resolution. With this purpose, Airborne Hyperspectral Scanner

(AHS) imagery from Madrid city center acquired during the DESIREX 2008 campaign [7] is used. Showing the relatively high performances of TRUST on this extremely challenging case where the spatial resolution and the number of bands are degraded, and where the studied scene is the city center of Madrid, opens the door to a large number of applications for this methodology. In addition, TRUST performances have been studied on both daytime and nighttime images of Madrid city center. Finally a new method, called TRUST Day and Night Synergy (TRUST-DNS), based on TRUST, has been developed to take advantage of the combination of daytime and nighttime images. It has been shown that TRUST-DNS improves the performances of TRUST.

This article is structured in 6 sections. In section 2 the DESIREX data used in this study is exposed. Then, in section 3 TRUST and its improved version TRUST-DNS are presented. In section 4, first, the pure material emissivity spectra and temperatures are defined, second, a calibration of TRUST and TRUST-DNS is performed to apply them on Madrid city center AHS images and finally the abundances and temperature retrieval performances of TRUST-DNS and TRUST on day and night images are compared. These results are discussed in section 5. The article finishes in section 6 with some conclusions and perspectives.

2. DESIREX 2008 Dataset

2.1. Data description

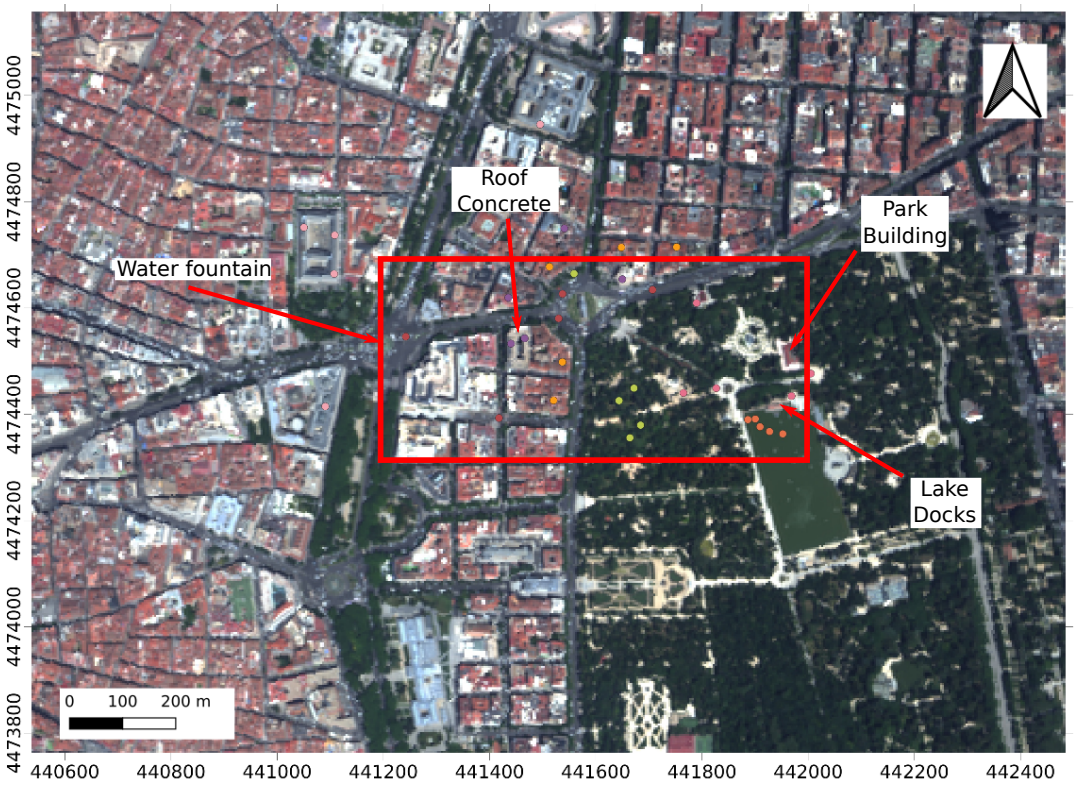

Figure 1. AHS image of Madrid city center from the 4th of July. RGB colours have been composed with AHS reflective bands 7, 4 and 1. The red square delimits the studied area. Colour dots indicate the position of the pixels used to define pure materials in the TRUST methodology, see section 3.

During the DESIREX 2008 experiment campaign over the city of Madrid, airborne hyperspectral scanner (AHS) data was acquired with a 4m spatial resolution over 80 spectral channels (0.443–13.4 μm) at several dates from 25th of June to 4th of July (summer) [7,16,17], see figure 1. From these 80 spectral channels, 10 are in the thermal domain (8.2–13.4 μm), see table 1. Together with these aircraft hyperspectral images, atmospheric characterizations were performed each day. On one hand, temperature profiles from ground level to 25 km altitude, and atmospheric water vapor content were measured with soundings several times a day at three different locations. On the other hand, relative humidity and air temperature evolution were measured in 6 fixed masts located in rural, urban-medium and urban-dense spots. These atmospheric characterizations are used to correct the aircraft images from atmospheric effects.

Table 1. Spectral configuration of thermal AHS bands

AHS band	Wavelength center	FWHM
Band 71	8180 nm	370 nm
Band 72	8660 nm	390 nm
Band 73	9150 nm	410 nm
Band 74	9600 nm	430 nm
Band 75	10070 nm	420 nm
Band 76	10590 nm	550 nm
Band 77	11180 nm	560 nm
Band 78	11780 nm	560 nm
Band 79	12350 nm	480 nm
Band 80	12930 nm	490 nm

In addition, spectral reflectivity and emissivity of 12 urban surfaces were also measured during this campaign. This measures are used to perform a supervised land cover classification on the daytime aircraft image from the 4th of July, where the *Maximum likelihood* was used as a decision rule and 13 different training classes were defined (12 materials plus shadows). The classification was performed using at-sensor radiance measures from the 80 spectral bands of the AHS sensor at 4m resolution [18]. However, even if in urban environments 4m pixels are frequently composed of several materials, no mixed pixel class is allowed in this classification. In this paper, we focus on two images acquired during this date, one day-time (11:32) and one night-time (22:14). The complete description of the dataset can be found in the DESIREX 2008 final report [7].

Finally, due to water absorption bands above 12000 nm [19], AHS bands 79 and 80 are not used in this article. In addition, the emissivity spectra of a large number of materials exhibit similar signatures at these wavelengths, rendering bands 79 and 80 not adapted to materials discrimination. Although [19] suggests to not use band 71, because of water absorption band below 8000 nm, due to the low performances when applying the method without band 71, it is kept in this study. The importance of band 71 when discriminating emissivity spectra of different materials is explained by the stronger signatures of these spectra at 8μm.

2.2. Scene description

Figures 2 a) and b) show, respectively, the zoomed RGB image of the studied area (day radiance image on 4th of July) and the corresponding classification map, both at 4m resolution. The scene contains a part of the *Retiro* park, mainly composed of vegetation and water (artificial lake), and the very heterogeneous

urban fabric located at the north-west of the park. In addition, some bare soil areas, a building with a roof made of red bricks and the lake docks are found in the park, a very particular building with a concrete roof is at the west of the park and a water fountain ("Cibeles") can be found in the west end of the image, see figure 1. In the scene, 6 classes of impervious materials are found and classified such as: Impervious road, Other road, Roofs with red bricks, Roofs asphalt, Roofs concrete, Roofs metal. In addition, two types of vegetation appear in the *Retiro* park, and also two types of water are discriminated (lakes and swimming-pools). Since, no mixed pixel class was allowed in the DESIREX classification, it is expected to have mixed pixels considered as pure ones, even at 4m resolution.

In the following, for the TRUST unmixing, we consider only one type of vegetation and one type of water since the emissivity spectra of both couples of vegetation and water are indistinguishable. Furthermore, since TES does not provide good descriptions of metallic surface temperatures and emissivities, only 5 impervious materials are considered: roads made of asphalt, roofs made of asphalt, other roads, roofs made of cement and roofs made of red bricks. However, while pixels initially classified within the two water and the two vegetation classes are now merged in only one water and one vegetation classes, pixels classified as "Roofs made of metal" maintain its status in the classification, but they are not considered when TRUST performances are analysed. Then, in the studied area a total of 7 materials are considered.

Thus, this Madrid city center scene is used to illustrate the application of the presented methodology along the article. For this purpose, both the classification and the radiance images are undersampled to 8m resolution in order to have a reference at 4m, see figure 2 c) and d). This undersampled classification produces a new class (mixed pixels) in the classification map at 8m resolution. Pixels at 8m are considered mixed in the new classification if the four 4m-pixels composing them do not belong to the same class.

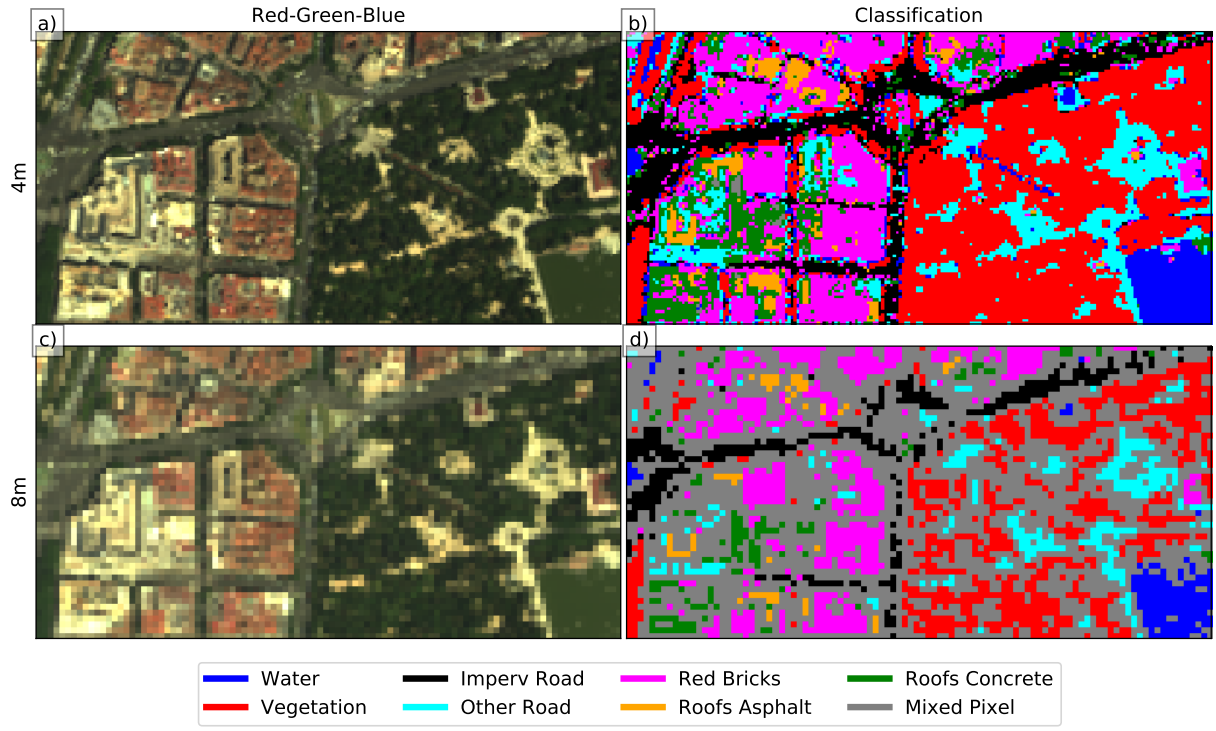

Figure 2. Left) RGB AHS images of Madrid city center at 4m (a) and 8m (c) resolutions. Right) DESIREX classification map at 4m resolution (b) and undersampled classification map at 8m (d).

3. Methodology

The proposed methodology, called TRUST-DNS, is an improvement of TRUST method, developed by Cubero Castan et al. 2015 [10], by taking advantage of Day-Night synergy, see figure 3. This section explains the different steps of TRUST-DNS in analogy with [10] for TRUST and indicating the main differences between TRUST and TRUST-DNS.

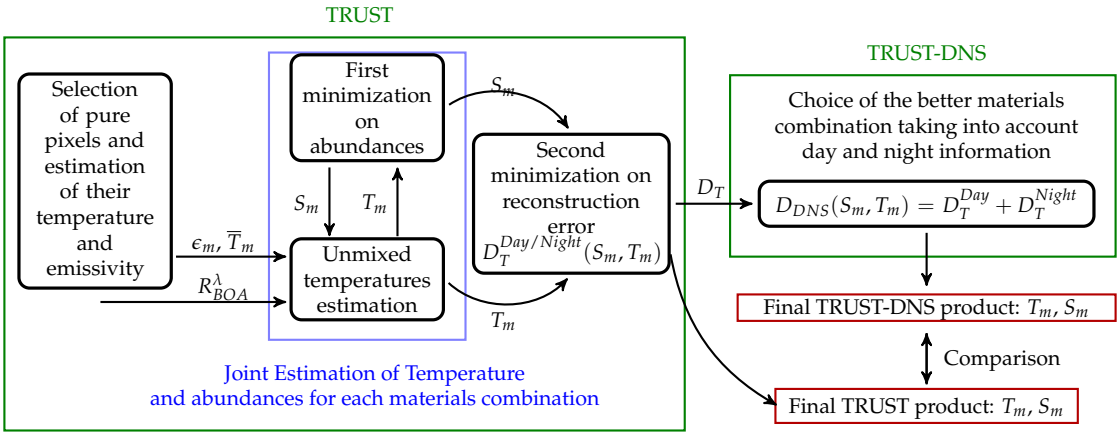

Figure 3. TRUST-DNS methodology diagram.

3.1. Radiative Transfer Equations

Considering a thermal image with N spectral bands, the Bottom of Atmosphere (BOA) radiance of a given pixel at a given wavelength λ is:

$$R^{\lambda}_{BOA,meas} = \frac{R^{\lambda}_{sens} - R^{\lambda}_{atm,\uparrow}}{\tau^{\lambda}_{atm,\uparrow}} \tag{1}$$

where R^{λ}_{sens} is the at sensor level measured radiance, $R^{\lambda}_{atm,\uparrow}$ is the atmospheric upwelling radiance and $\tau^{\lambda}_{atm,\uparrow}$ is the upwelling transmittance.

On the other hand, for a flat-ground-scene, the resulting BOA radiance for a mixed pixel can be expressed as a linear mixture of radiances:

$$R^{\lambda}_{BOA} = \sum_{i=1}^{M} \left(\epsilon^{\lambda}_i \cdot B^{\lambda}(\overline{T}_i) + (1 - \epsilon^{\lambda}_i) \cdot R^{\lambda}_{atm,\downarrow} \right) S_i \tag{2}$$

where M is the number of materials composing the pixel, ϵ^{λ}_i is the emissivity of material i at wavelength λ, $\overline{T}_i$ is the mean temperature of material i in the pixel and $B^{\lambda}(T)$ is the Planck law at temperature T, $R^{\lambda}_{atm,\downarrow}$ is the atmospheric downwelling radiance, and S_i is the abundance of material i in the pixel. The abundance of material i in a pixel is defined as the fraction of the pixel covered by i. Thus for any pixel, the sum of the abundances of the materials composing it is normalized to one, $\sum_{i=1}^{M} S_i = 1$.

3.2. Selection of pure pixels and estimation of their temperature and emissivity

Pure pixels are manually selected using the classification map build from the 4th of July images at 4m resolution during the DESIREX 2008 campaign, see figure 1. From homogeneous areas on the classification map, five pixels far enough from the borders are selected to represent each pure material or endmember. Avoiding pixels from the borders of the homogeneous areas allows to reduce errors due to misregistration

between the classification map and the AHS (day and night) images, as well as errors due to classification accuracy (at these resolutions, interfaces between homogeneous areas are considered to be mixed, even if the classification ignores this possibility).

Thermal and Emissivity Separation (TES) method [10,20] is used on each pure pixel to obtain its temperature and emissivities. TES needs atmospheric correction but contrary to other methodologies such as Split-Window or Mono-Window methods, it allows to estimate both the temperature and emissivities of the pixel. TES is based on a three-step approach: Normalized Emissivity Method (NEM), Ratio, and Maximum and Minimum Difference (MMD) [20].

The mean temperature $\overline{T_i}$ and emissivities ϵ_i^λ of each endmember are then defined as the mean of the temperatures and emissivities measured for the five pixels identifying each material. Hence, this choice is extremely important since, even if the five selected pixels characterizing a material are pure, 3D structures and shadows (abundant in cities) can alter the obtained temperatures and spectra. Thus, the pure pixel selection should be considered as strongly influencing the methodology performances.

3.3. Joint Estimation of Temperatures and Abundances

Given a mixed pixel made of M materials, TRUST allows the joint estimation of temperatures and abundances from an iterative process (material emissivities are considered to be well defined from pure pixels and to remain constant in the image). TRUST has been already tested with a maximal value of $M = 2$ and $M = 3$, *i.e.* allowing combinations of until two and three materials per pixel [15]. Thus, Cubero-Castan 2014 shows that TRUST performances are higher allowing sets of until 2 materials per pixel ($M = 2$) [15].

Then, the iterative process starts by estimating the abundances for any possible set of materials with the minimization of the reconstruction error of the BOA radiance:

$$D(\mathbf{S}) = \sqrt{\frac{1}{N}\sum_{\lambda=1}^{N}\left(R^\lambda_{BOA,meas} - R^\lambda_{BOA}(\mathbf{S},\mathbf{T})\right)^2} \tag{3}$$

where $\mathbf{S}$ are the abundances of the set of materials composing the mixed pixel, $\mathbf{T} = \overline{\mathbf{T}} + \mathbf{\Delta T}$ are the temperature of the materials in the pixel defined as the mean temperature of the material plus $\mathbf{\Delta T}$, whose estimation depends on $\mathbf{S}$. For this first iteration abundance estimation $\mathbf{\Delta T} = 0$.

Then, once the abundance S_i of each material within the pixel is known, only one hypothesis is required to estimate the temperatures in the mixed pixel: the temperature of every material composing the pixel is close to the corresponding mean temperature of the material. In order for this hypothesis to be correct, it is preferable to work on small images, since the material temperatures can strongly vary between far locations. Thus, this hypothesis allows to linearize the black body law $B^\lambda(T_i)$ around the mean temperature $\overline{T_i}$. Then, following the first-order Taylor series approximation of eq.(2), the centered radiance is:

$$\begin{bmatrix}\Delta R_{\lambda_1}\\ \vdots \\ \Delta R_{\lambda_N}\end{bmatrix} = \begin{bmatrix} A_{\lambda_1}^{\overline{T_1}} & \cdots & A_{\lambda_1}^{\overline{T_M}} \\ \vdots & \ddots & \vdots \\ A_{\lambda_N}^{\overline{T_1}} & \cdots & A_{\lambda_N}^{\overline{T_M}}\end{bmatrix} \begin{bmatrix}\Delta T_1\\ \vdots \\ \Delta T_M\end{bmatrix} \equiv \mathbf{\Delta R} = \mathbf{A}\cdot\mathbf{\Delta T} \tag{4}$$

with the centered radiance $\Delta R_{\lambda_j} = R^{\lambda_j}_{BOA}(T_i) - R^{\lambda_j}_{BOA}(\overline{T_i})$, $\Delta T_i = T_i - \overline{T_i}$ and $A_{\lambda_j}^{\overline{T_i}} = \epsilon_i \cdot S_i \cdot \frac{\partial B^{\lambda_j}(T)}{\partial T}|_{\overline{T_i}}$. The number of bands N defines the number of equations and the number of materials per pixel M defines the

number of unknowns. So, for the system of equations to be determined N should be greater or equal than M.

Finally, the linear unbiased estimator minimizing the variance of the estimation is [21]:

$$\mathbf{\Delta T} = (\mathbf{A^t} \cdot \mathbf{C^{-1}} \cdot \mathbf{A})^{-1} \cdot \mathbf{A^t} \cdot \mathbf{C^{-1}} \cdot \mathbf{\Delta R} \tag{5}$$

where $\mathbf{C}$ is the noise covariance matrix.

Once $\mathbf{\Delta T}$ is estimated, eq.(3) is newly minimized, with $\mathbf{T} = \overline{\mathbf{T}} + \mathbf{\Delta T}$, to find $\mathbf{S}$. Thus for each possible combination of pure materials composing the mixed pixel, this iterative process aims at estimating the abundances and temperatures minimizing eq.(3).

A second minimization is needed to distinguish which combination of materials (among the tested sets) composes the mixed pixel. With this purpose a new cost function is introduced:

$$D_T(\mathbf{S}) = D(\mathbf{S}) + \gamma \sqrt{\frac{1}{M} \cdot \sum_{i=1}^{M} (\Delta T_i)^2} \tag{6}$$

where γ is an hyperparameter weighting the significance of ΔT in the minimization. The choice of γ is very important, since small values will give more significance to emissivity differences, while for high values the methodology will look mainly for material combinations with $\mathbf{\Delta T} \approx 0$.

Thus, TRUST selects the set of materials minimizing $D_T(\mathbf{S})$ with the optimal temperatures and abundances minimizing $D(\mathbf{S})$ as the one composing the mixed pixel.

3.4. Day and Night Synergy: TRUST-DNS

In oder to take advantage of possible synergies between day and night images, the above TRUST methodology has been slightly modified. TRUST is applied separately on day and night images with normalized cost functions:

$$D^j(\mathbf{S}) = \sqrt{\frac{1}{N} \sum_{\lambda=1}^{N} \left(\frac{R^{\lambda}_{BOA,meas} - R^{\lambda}_{BOA}(\mathbf{S},\mathbf{T})}{R^{\lambda}_{BOA,meas}} \right)^2} \quad \text{with } j \equiv \text{Day or Night} \tag{7}$$

$$D^j_T(\mathbf{S}) = D^j(\mathbf{S}) + \gamma \sqrt{\frac{1}{M} \cdot \sum_{i=1}^{M} (\frac{\Delta T_i}{\overline{T_i}})^2} \quad \text{with } j \equiv \text{Day or Night} \tag{8}$$

where D^{Day} and D^{Night} are estimated for each pixel on the same combinations of materials. Finally, the set of materials composing the mixed pixel is defined as the one minimizing $D_{DNS} = D_T^{Day}(\mathbf{S}) + D_T^{Night}(\mathbf{S})$.

The normalization of the cost functions is needed to give the same weight to the information coming from day and night images independently of their radiance and temperatures absolute values. Abundances and temperatures are allowed to vary for the same mixed pixel between day and night. This is expected for temperatures but not for abundances which are supposed to remain constant. However, due to possible registration errors and viewing angles discrepancies, we decided to not impose the same abundances to the day and night mixed pixels.

3.5. Evaluation criteria

The performances of TRUST-DNS for retrieving abundances in a given scene are evaluated differently for the mixed (δS_{mixed}) and the pure (δS_{pure}) pixels composing the scene [15]. Thus for pure pixels, the abundance error of material m is evaluated on pixels where $S_m = 1$ by looking at the unmixed value of

S_m. On the other hand for mixed pixels composed of a materials combination, the abundance of materials which are not within this combination must be $S_i = 0$, and then the abundance error is estimated by looking at the unmixed values S_i of materials which are not in the combination. For temperature retrieval performances (δT), mixed and pure pixels are not discriminated.

$$\delta S_{pure} = \sqrt{\frac{\sum_m \sum_{k\ pure\ m} (S_{k,m} - \hat{S}_{k,m})^2}{N}} \tag{9}$$

$$\delta S_{mixed} = \sqrt{\frac{\sum_m \sum_{k\ mixed\ without\ m} (\hat{S}_{k,m})^2}{N}} \tag{10}$$

$$\delta T = \sqrt{\frac{\sum_k \left[T_k - (\sum_m \hat{S}_{k,m} (\hat{T}_{k,m})^4)^{1/4}\right]^2}{N}} \tag{11}$$

where k sums over the pixels and m over the materials in each pixel, and N is the total number of pixels taken into account. $\hat{S}$ ($\hat{T}$) indicates the estimated unmixed abundance (temperature), while S (T) indicates the reference abundance (temperature). For abundances, the used reference is the classification at 4m from which a reference abundance map at 8m is generated. The ratio between the classification and the abundance map resolutions (4m and 8m respectively) leads to limitations in the abundance retrieval performances study, since the reference map only presents very discretized abundances (0%, 25%, 50%, 75% and 100%). For temperatures, the reference is the TES measured temperature at 8m.

4. Results

This section compares the performances of TRUST-DNS and TRUST applied separately on day and night images, when estimating abundances and temperatures over a heterogeneous urban scene. The chosen urban scene, Madrid city center, is considered to be mainly composed of 7 materials. The mean temperatures ($\overline{T_m}$) and emissivities (ϵ_m) of each one of these materials are defined as the mean of 5 manually chosen pixels (see figure 1). For the unmixing, each pixel in the scene is considered to be composed of no more than 2 materials. This choice allows to reduce computation time and also to reduce errors in unmixing [15]. Since TRUST has been shown to outperform other thermal unmixing techniques before [10,15], this work focuses on comparisons between TRUST applied on day and night images and TRUST-DNS.

4.1. Characterization of endmembers

Figures 4 a) and b) show the endmembers emissivities obtained with TES on day and night images respectively. Every spectra present emissivity values between 0.86 and 0.98. Moreover, for any pure material, differences are found between day and night emissivity spectra, with a tendency, mainly for lower wavelengths (<9.7 μm), to overestimate day emissivities compared to night ones. These differences are at most of 2% of emissivity.

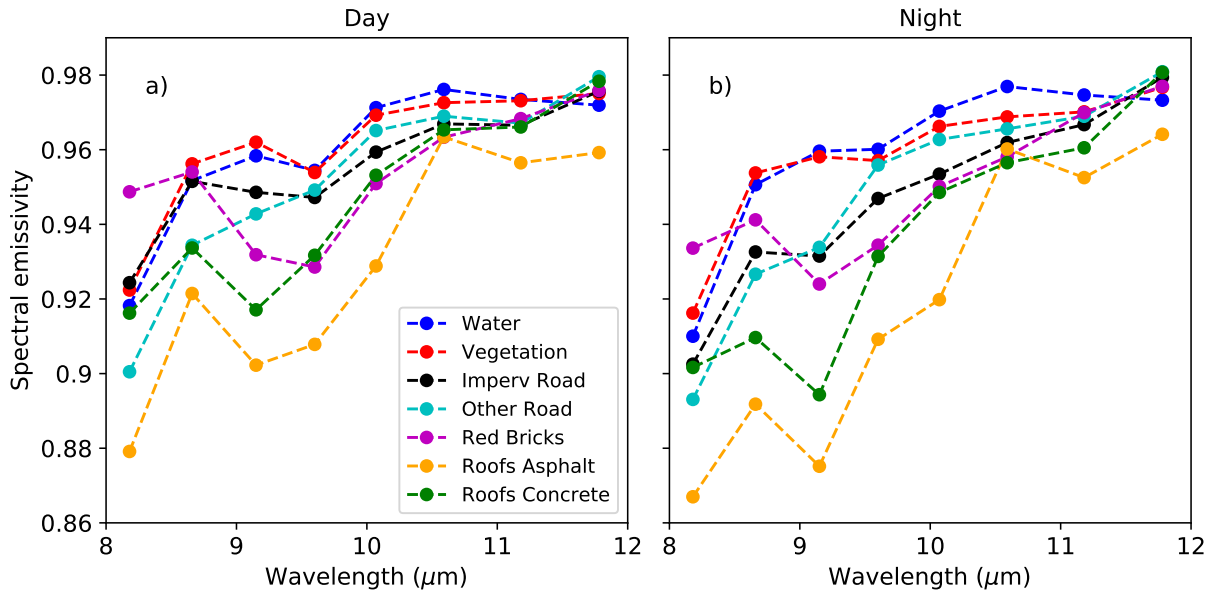

Figure 4. Emissivity spectra of pure materials found in the studied area, obtained with TES over day (a) and night (b) images.

Table 2 shows the endmembers mean temperature for day and night. As expected, day temperatures are higher, and more important contrasts between day and night temperatures are found for impervious materials such as Asphalt, Concrete and Red bricks than for natural materials such as water or vegetation. The obtained temperatures are within the expected range for sun exposed materials during summer with day temperatures between 25 and 50 ^{o}C and night temperatures between 18 and 25 ^{o}C.

Table 2. Mean temperatures ($\overline{T_m}$) of pure materials found in the studied area with TES over day and night images.

Material	Day mean temperature (K)	Night mean temperature (K)
Water	301	300
Vegetation	306	298
Roads Asphalt	324	305
Other Roads	315	300
Red bricks	323	296
Roofs Asphalt	331	293
Roofs Concrete	323	297

4.2. Study on the choice of γ

As explained in section 3.3, two terms are minimized in TRUST (TRUST-DNS). In the second one, the γ hyperparameter, which weights the importance of the temperature difference ($\mathbf{\Delta T}$) in the minimization, is introduced. In order to find the best value for γ a previous study should be performed. Based on [15] a set of γ values, from $\gamma = 10^{-4}$ to $\gamma = 1$, is tested for TRUST applied on the day and night images separately and for TRUST-DNS. The analysis of unmixing performances in function of γ is based on abundance

errors from eq.(9) and eq.(10), which measure the pixel fraction difference between the classification and the unmixing results, and temperature error from eq.(11), which measures the temperature difference in K between the unmixed temperature map and the TES temperatures at 8m of resolution, see figure 5. In every case, abundance errors for pure pixels obtained with eq.(9) are between 0.4 and 0.8 and their minimal values are smaller for TRUST-DNS. Mixed pixel errors obtained with eq.(10) are around 0.2 and 0.3 and their minimal values are similar for TRUST and TRUST-DNS. Moreover TRUST-DNS appears less influenced by the choice of γ. On the other hand, temperature errors are around 0.3 and 0.6 K with similar minimal values for TRUST and TRUST-DNS on day but better performances of TRUST-DNS on night. Newly as for abundance errors, TRUST-DNS temperature errors are less influenced by the choice of γ. The choice of the best γ is done separately for the different studied cases. While for TRUST on the day image $\gamma = 0.01$ ($\log(\gamma) = -4.6$) minimizes the errors, for TRUST on night the best choice is $\gamma = 0.005$ ($\log(\gamma) = -5.3$), and for TRUST-DNS $\gamma = 0.5$ ($\log(\gamma) = -0.69$) is chosen for both day and night images. In the following sections, only results with these γ values are shown. Then, for TRUST on the day image $\delta S_{mixed} = 0.25$ and $\delta S_{pure} = 0.48$ of the pixel fraction, while $\delta T = 0.39$ K. For TRUST on the night image $\delta S_{mixed} = 0.24$, $\delta S_{pure} = 0.48$ of the pixel fraction and $\delta T = 0.33$ K. Finally, for TRUST-DNS on both day and night image $\delta S_{mixed} = 0.24$ and $\delta S_{pure} = 0.43$ of the pixel fraction while for daytime $\delta T = 0.40$ K and for nighttime $\delta T = 0.29$ K.

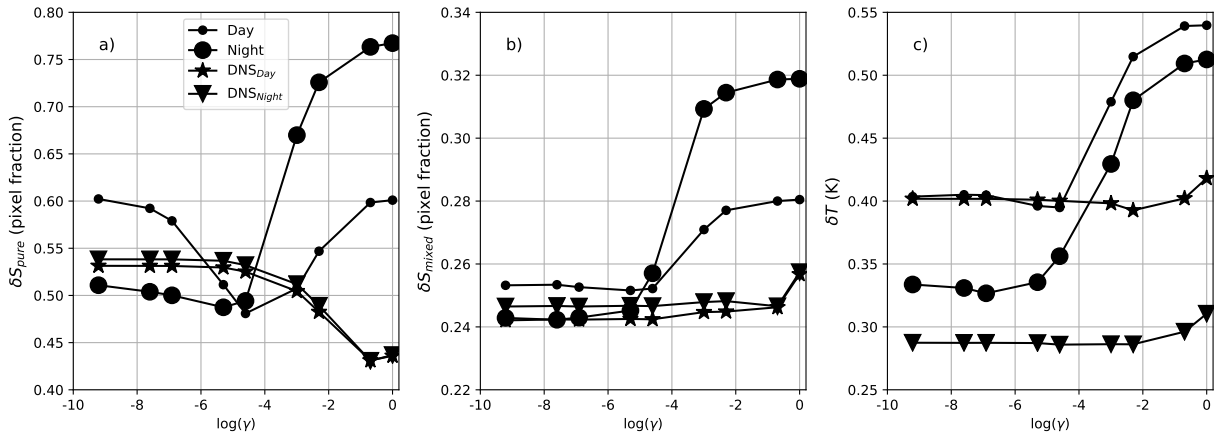

Figure 5. Abundance errors on pure pixels δS_{pure} (a), on mixed pixels δS_{mixed} (b), and temperature errors δT (c). All the three in function of the logarithm of the hyperparameter γ, and for TRUST on day image, TRUST on night image, TRUST-DNS on day image and TRUST-DNS on night image.

4.3. Abundances retrieval

Figures 6, 7, 8 and 9 show the abundances retrieved for each material together with the DESIREX classification at 8m. Figure 6 shows the abundances retrieved with TRUST on the day image, figure 7 with TRUST on the night image, figure 8 with TRUST-DNS on the day image and figure 9 with TRUST-DNS on night.

Thus, TRUST on day image (figure 6) allows to recover some pure regions of water pixels as well as pure regions of vegetation, roads with asphalt, other roads and red bricks pixels which are in agreement with the pure regions of the classification. Trees and the water fountain in the avenues, as well as the lake docks, the building and some soil surfaces in the park are also found. However, pixels with water are found everywhere in the image, maybe due to shadow effects. In addition, mixed pixels are also found in agreement with the DESIREX classification. TRUST on night (figure 7) shows worst performances when

finding water: no pure pixels are found in the park lake, and the water fountain is lost. In addition, *other roads* pure pixels are also lost, and vegetation pixels in the avenues appear as mixed ones. TRUST-DNS allows to reduce noise and to find more pure pixels both on day and night images (figures 8 and 9). Thus, the lake and its docks are perfectly defined, as well as the park vegetation, its small soil surfaces and its building, and the water fountain in the avenues. In addition, mixed pixel regions are found at the interfaces of pure regions: between the park and the avenues around, in the limits of the lake docks and also in the borders of the park building. Only some small differences are found between TRUST-DNS day and night, as expected since for both the materials composing a given pixel are the same. With every method and image, a square roof of concrete is found. Visually it is possible to verify the existence of this roof. However, in the DESIREX classification it was misclassified and confused with *other roads* material. Also in any case, the material *Roofs asphalt* appears as negligeable. Only tens of pixels are identified to contain this material, and they are scattered in the right hand side of the image. In general, TRUST and especially TRUST-DNS, recovers the mixed and pure areas found on the DESIREX classification.

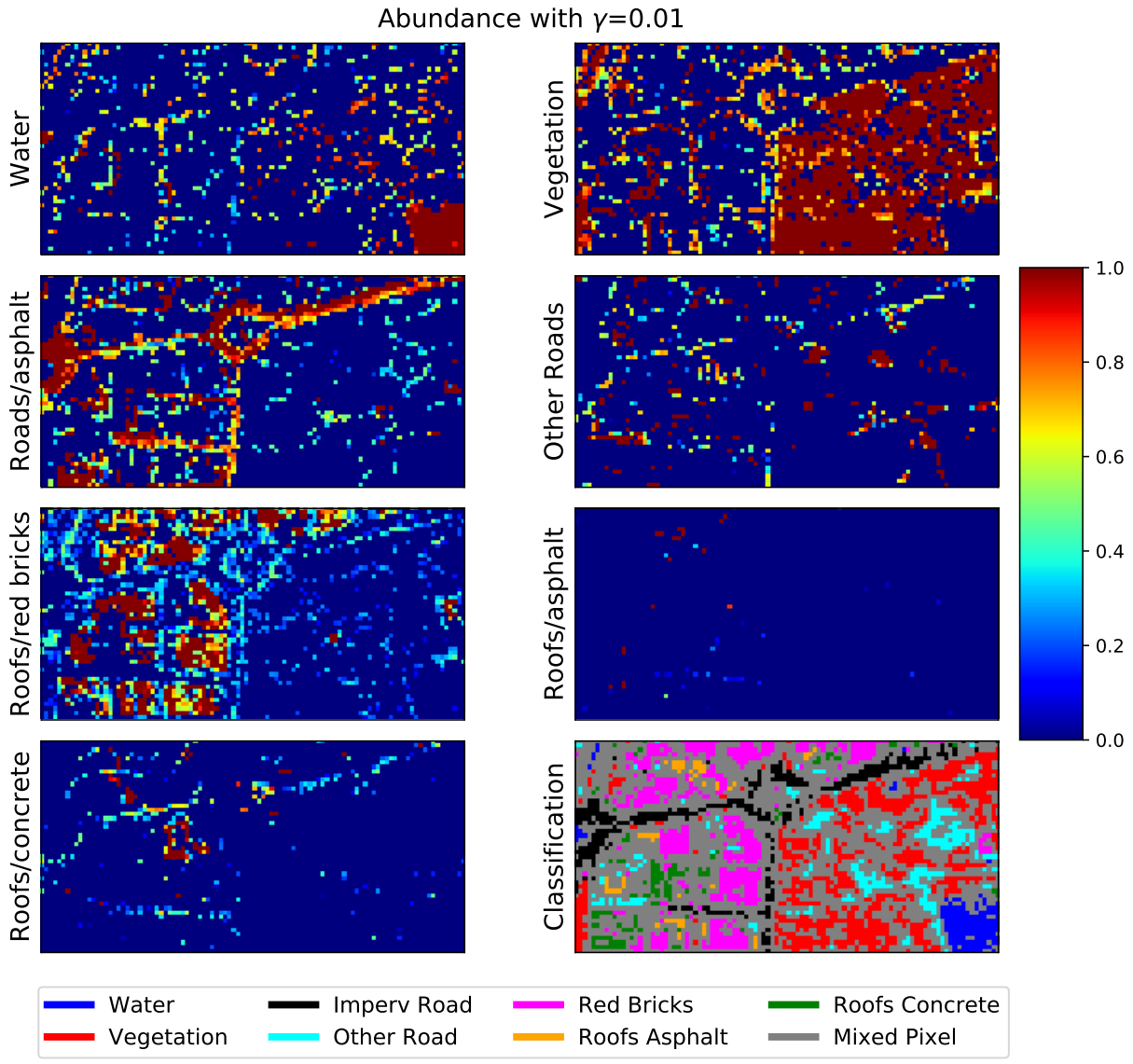

Figure 6. TRUST day abundances map at 8m for each considered material together with the DESIREX classification undersampled at 8m.

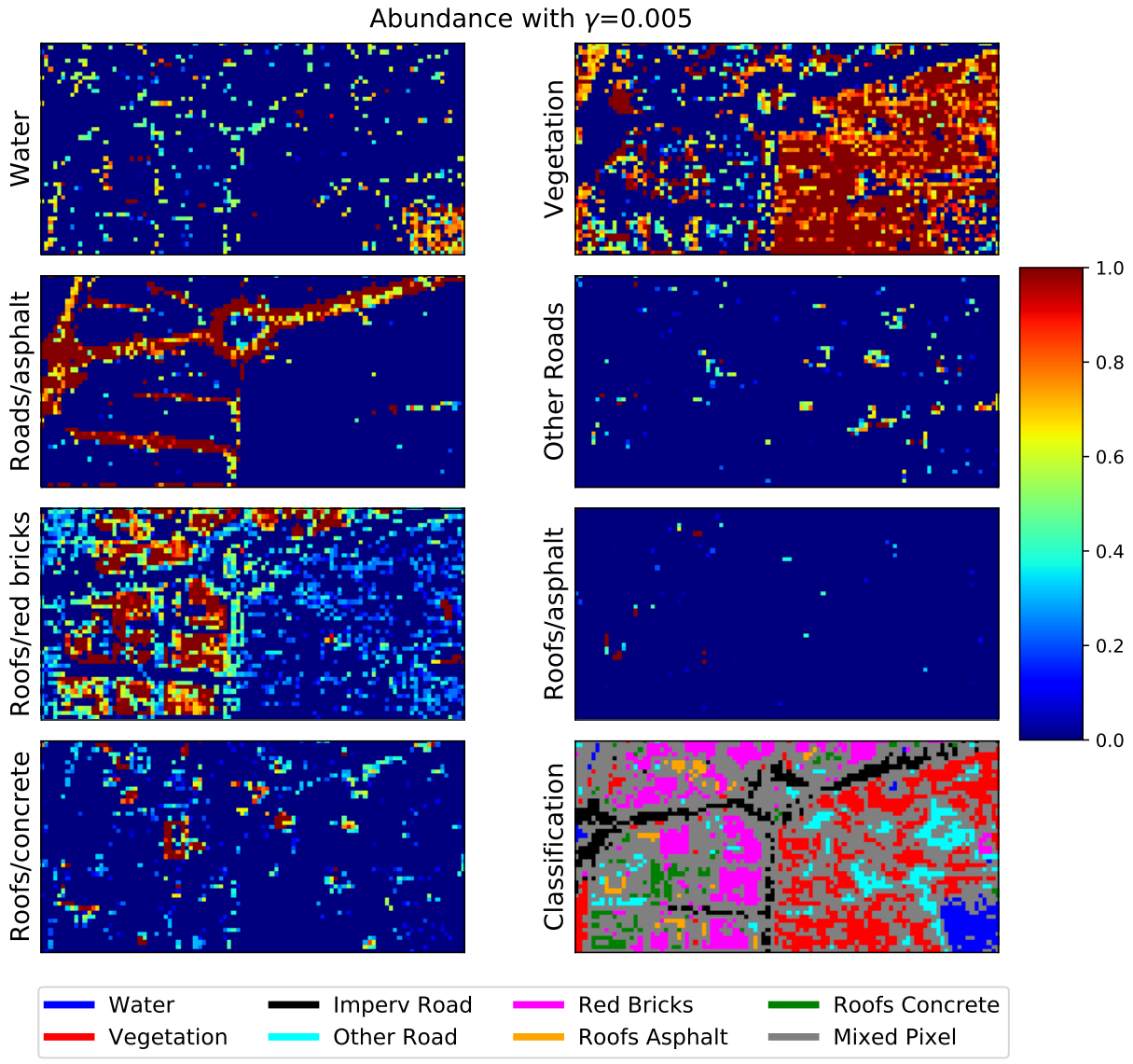

Figure 7. TRUST night abundances map at 8m for each considered material together with the DESIREX classification undersampled at 8m.

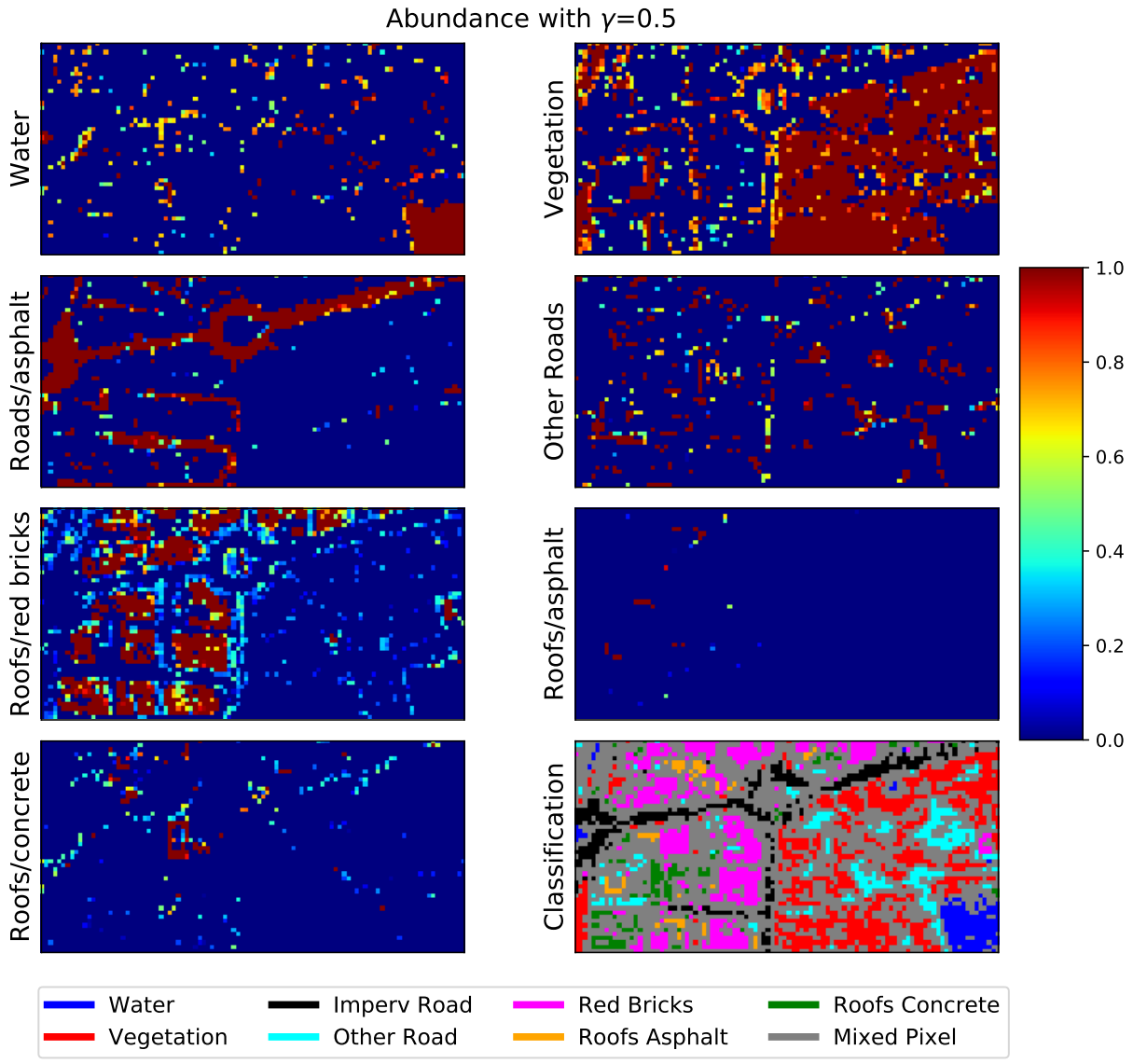

Figure 8. TRUST-DNS day abundances map at 8m for each considered material together with the DESIREX classification undersampled at 8m.

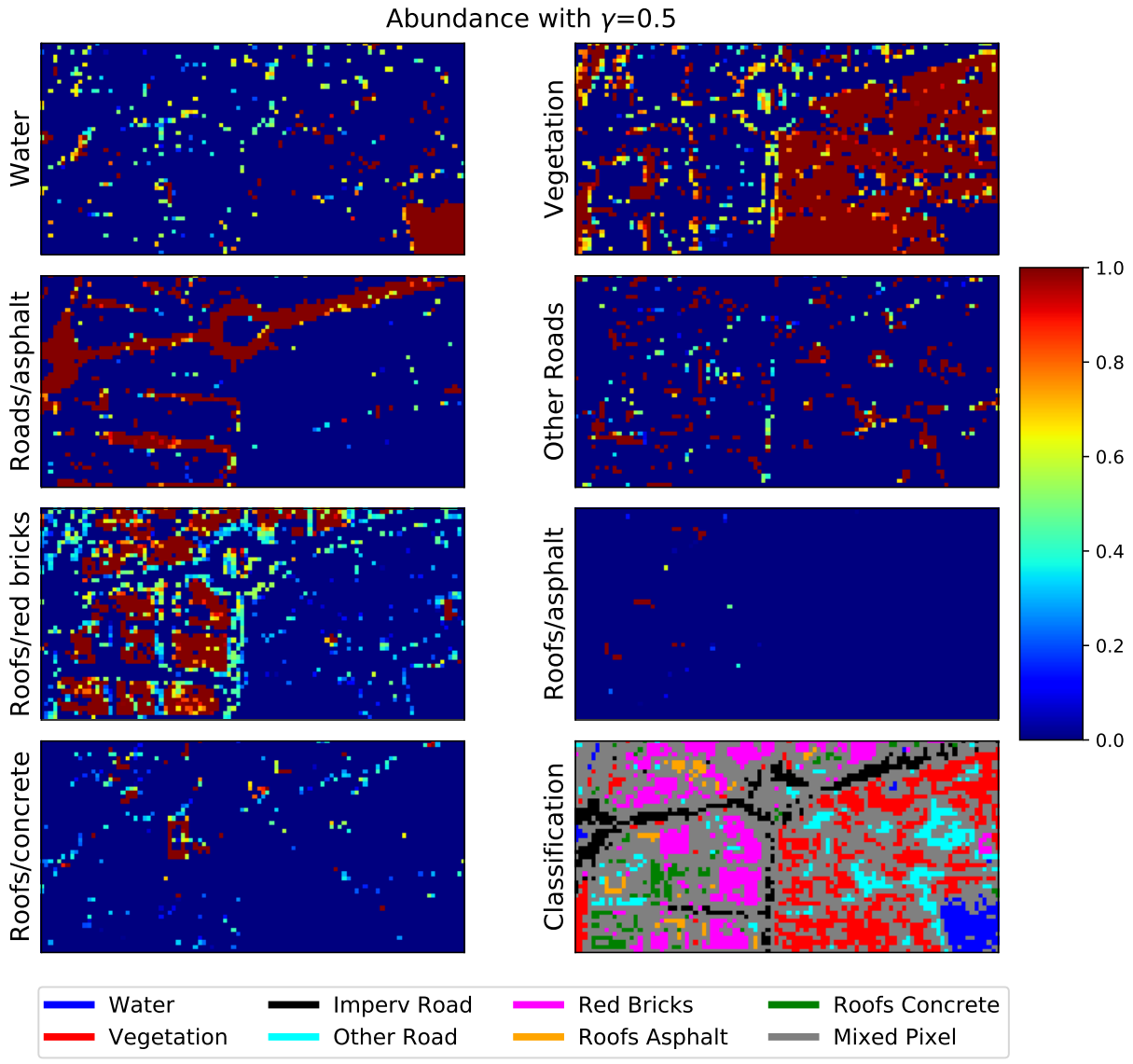

Figure 9. TRUST-DNS night abundances map at 8m for each considered material together with the DESIREX classification undersampled at 8m.

4.4. Temperature retrieval

Figures 10, 11, 12 and 13 show the temperatures retrieved for each material together with the TES temperature at 8m. Hence, TRUST applied on thermal images allows to link urban materials to LSTs without needing a previous land cover classification. Figure 10 shows the temperatures retrieved with TRUST on the day image, figure 11 with TRUST on the night image, figure 12 with TRUST-DNS on the day image and figure 13 with TRUST-DNS on night. For both day temperature images (figures 10 and 12), and for both pure and mixed pixels, impervious materials *roads asphalt and red bricks* present the highest temperatures, and natural materials such as water, vegetation and soil (*other roads*) present lower temperatures. Thus, showing that manmade materials lead to an increase of LST during day which is mitigated by vegetation or water. TRUST and TRUST-DNS exhibit similar performances for

day image temperature retrieval. On the other hand, for both night images *Roads Asphalt* presents the highest temperatures, followed by water and soil, and with roofs and vegetation exhibiting the lowest temperatures. Then during night, the canyon structure drives the LST spatial distribrution, with roofs being cooler and roads being hoter. In addition, vegetation and soil does not seem to lead to cool LSTs. TRUST-DNS on night present less noisy results than TRUST, maybe because of the better performances in abundance retrieval.

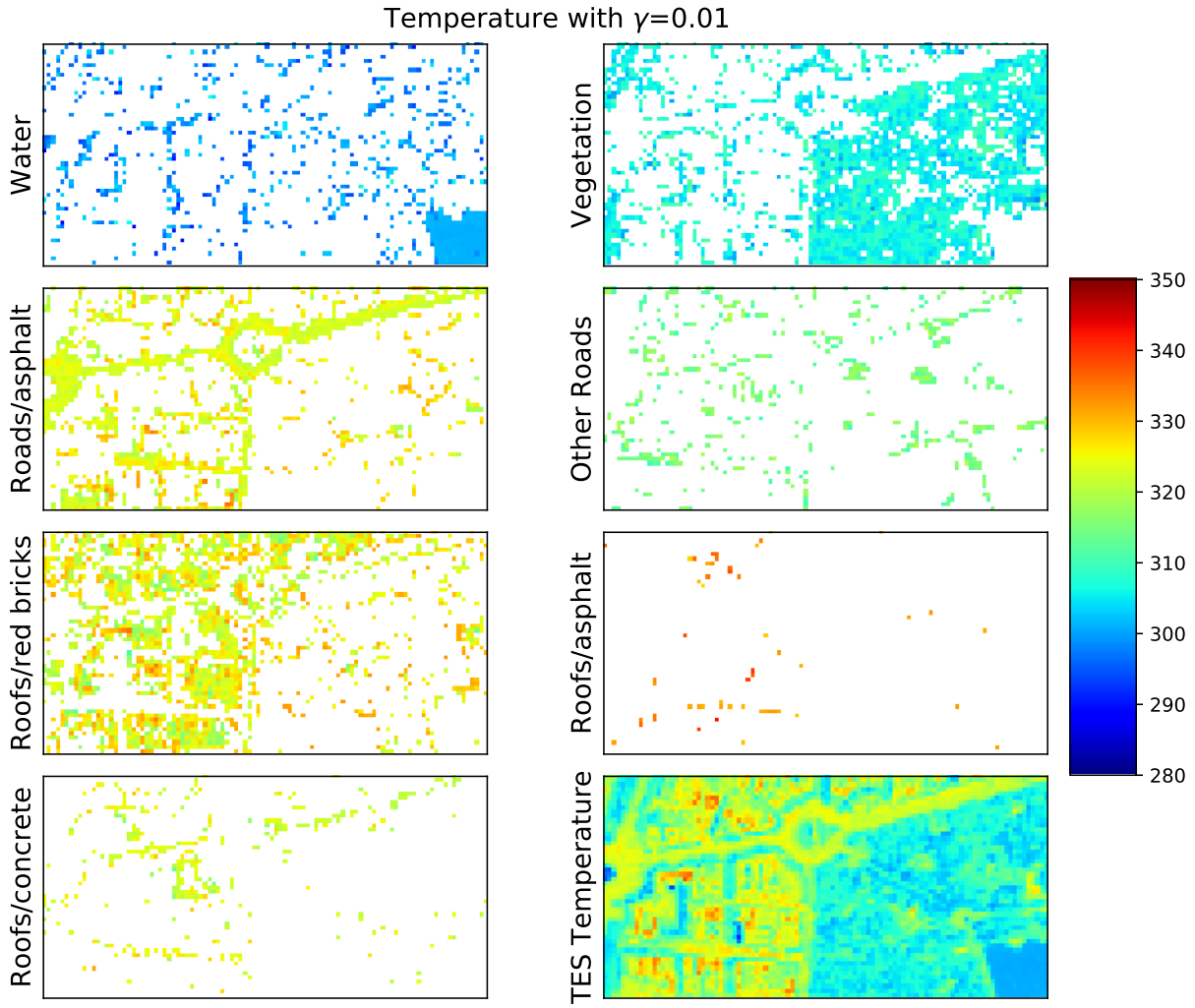

Figure 10. TRUST day temperatures map at 8m for each considered material together with the TES temperature at 8m.

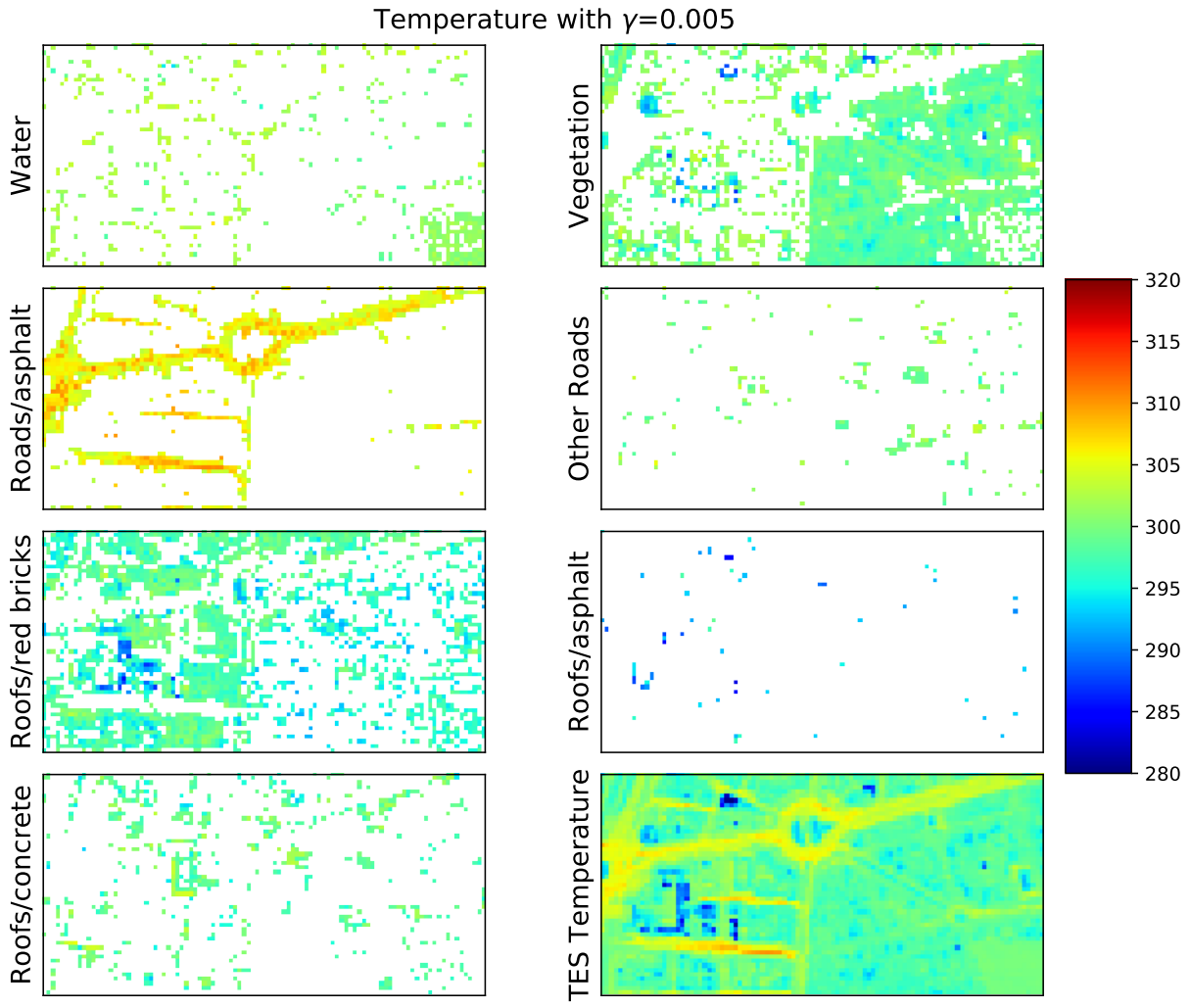

Figure 11. TRUST night temperatures map at 8m for each considered material together with the TES temperature at 8m.

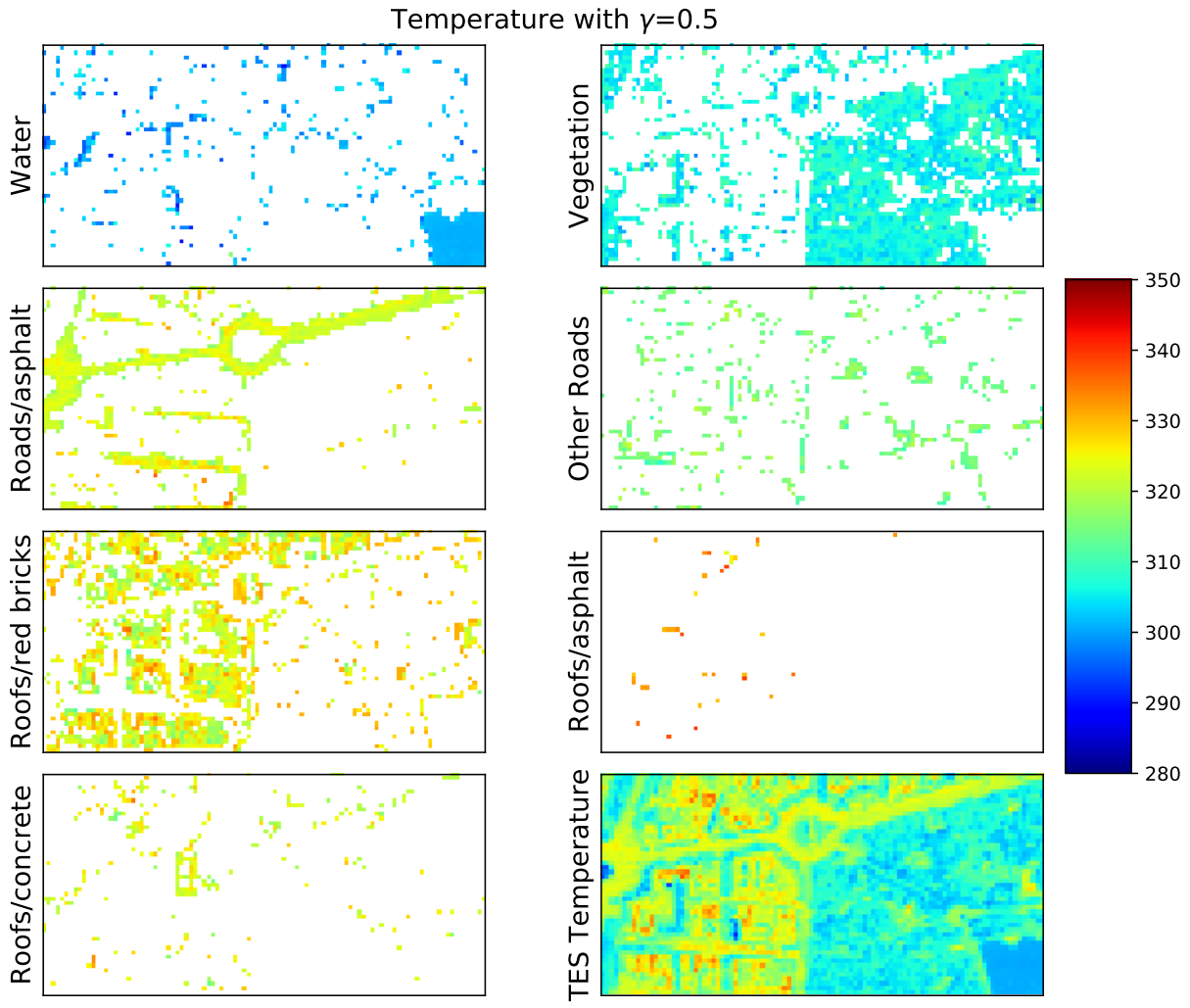

Figure 12. TRUST-DNS day temperatures map at 8m for each considered material together with the TES temperature at 8m.

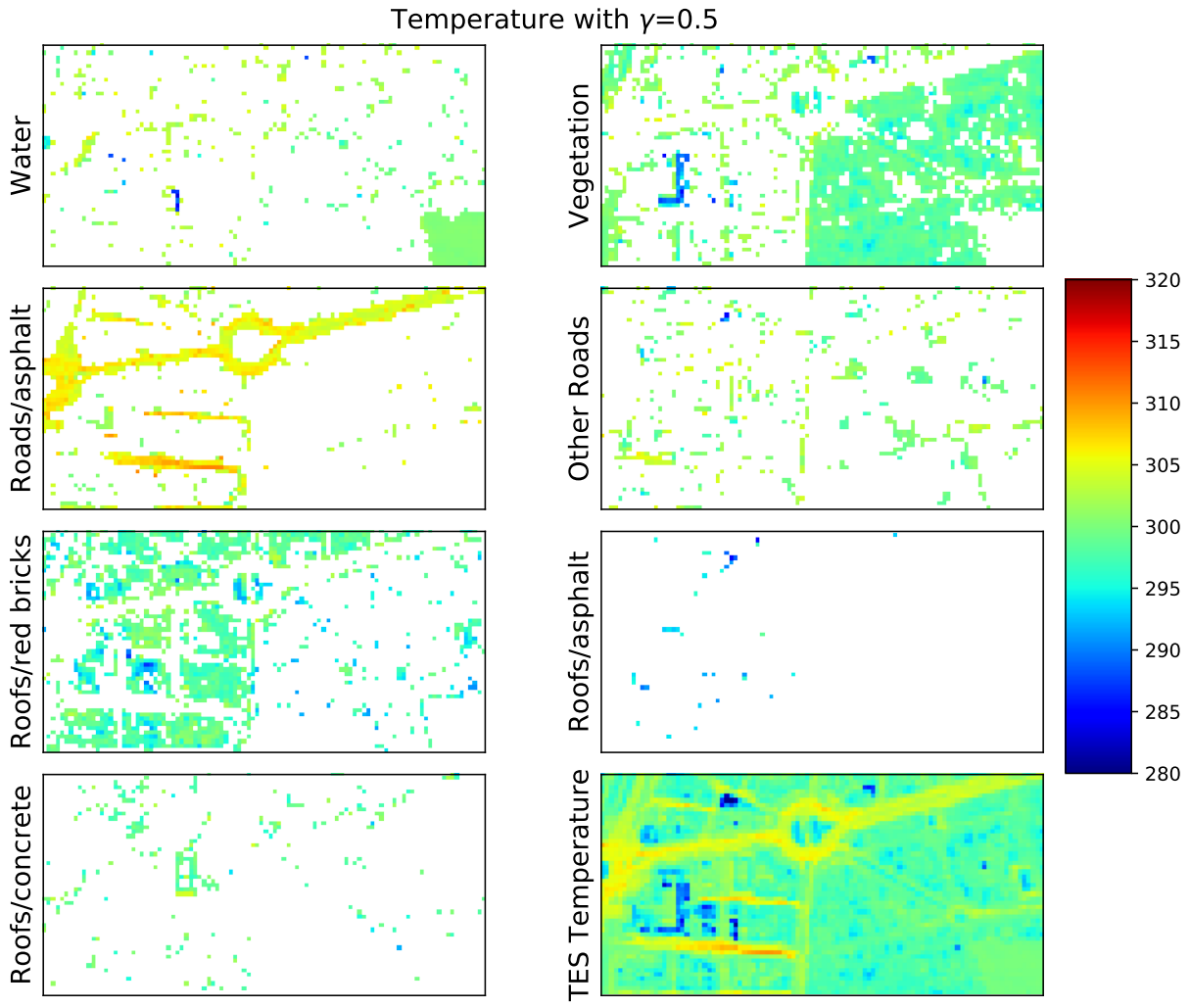

Figure 13. TRUST-DNS night temperatures map at 8m for each considered material together with the TES temperature at 8m.

5. Discussion

This article shows the potentiality of TRUST and TRUST-DNS to perform high spatial resolution studies of urban LSTs. Moreover, TRUST and TRUST-DNS allow to link manmade and natural materials to different temperature behaviors, and then appear as powerful tools for the characterization and understanding of SUHIs at high spatial resolution. In addition, several methodological aspects of TRUST (TRUST-DNS) can be tuned to improve its performances in function of the city structural and material characteristics. It is also important to take into account that in this study only 8 thermal spectral bands were used, while in previous TRUST studies no less than 32 bands were used. Of course, the more spectral bands there are, the better the performance [15], and so this study places the methodology at the limits of its applicability.

Endmembers definition in the thermal domain

The ideal number of endmembers defined to unmix a given scene strongly depends on the scene and the image resolution. Thus, the number of pure materials should increase when the scene heterogeneity

and/or the image resolution increase. However, considering too many pure materials leads to a decrease in unmixing performances, since the number of possible material combinations increases exponentially with the number of endmembers, inducing innacuracies in the minimization of the radiance reconstruction. Having a previous classification at a slightly better resolution than the initial one (in this case the previous classification at 4m and the radiance images at 8m), allows to recognise the number of endmembers which is adapted to the scene and resolution. Furthermore since DESIREX classification was done with 80 reflective and thermal bands and we have only 8, we decided to slightly decrease the number of pure materials defined in the DESIREX classification. Thus, from the two water and two vegetation classes, only one is retained to define each class. In addition, since TES presents low performances on metallic materials [20], "Roofs made of metal" class is not used.

Furthermore, different methodologies can be used to define the emissivity spectra and mean temperature of endmembers. In this work, and based on [10,15], five pure pixels in the image are manually selected to define each pure material. Indeed, as recommended by [7,10,19] TES algorithm is used on both day and night images to obtain the emissivity spectra and temperature of each manually selected pixel. However, emissivity differences between day and night pixels are found, see figure 4. These differences are lower or equal to 2% of emissivity, which is within the range of the TES emissivity retrieval accuracy (1.5% was found in Gillespie et al. 1998 [20] and 3% in Oltra-Carrio 2013 [19]). Small co-registration errors and or viewing angles differences between day and night images can also explain these small differences between day and night pure material spectra. In addition, atmospheric reflective contribution, which is more important during day, can be misestimated, influencing the emissivity characterization. A slight trend to small values at short wavelengths is also observed, especially for night emissivities. This may be partially explained by the 8 μm band to be slightly influenced by water absorption bands below 8 μm. Atmospheric water vapour content during 4th of July acquisitions was 1.5 $g\,cm^{-2}$ during day and 2.5 $g\,cm^{-2}$ during night [7].

TRUST and TRUST-DNS performances

TRUST-DNS appears as more stable than TRUST when dealing with γ variations. In addition, the study on the choice of γ showing the global unmixing errors compared to DESIREX classification for abundances and TES at 8m for temperatures, illustrates that once the most performant γ is chosen, TRUST-DNS performs better than TRUST on both abundance and temperature retrieval.

However, these results should be analyzed carefully. On the one hand, the 4m classification used as reference for the material abundances study does not include a mixed pixel class, even if at this resolution in urban environments mixed pixels appear. Then, having the DESIREX classification as reference induces inaccuracies, mainly in the pure pixel abundance errors. This effect is observed in figure 5, where pure pixel abundance errors are double compared to those of mixed pixels, *i.e.* TRUST correctly finds mixed pixels where the classification considers pure ones, leading to an increase in the pure pixels abundance errors. Hence, having a higher resolution classification of the studied area as reference would allow to go deeper in this study. Another option to advance in this study is to perform a new 4m classification with a likelihood threshold in the *Maximum likelihood* criteria, to consider mixed pixels. On the other hand, the resolution ratio between the classification used as reference and the unmixed image, being only of two, limits the abundance error quantification, since reference abundances are restricted to few discretized values (0%, 25%, 50%, 75% and 100% of the pixel) while TRUST (TRUST-DNS) abundances can take any value in [0%, 100%] range. However, greater ratios such as the 16m/4m one are not intended for the moment, since TRUST performances were strongly degraded when it was applied on lower resolution images (TRUST applied on 16m resolution images of Madrid city center was tested within the framework of this work).

Thus, even if it is difficult to know which abundance map is better, since no accurate information is available (reference at 4m), TRUST-DNS seems to better delineate urban objects such as streets, buildings, the park lake or vegetated areas. Thus, TRUST-DNS improves abundance retrieval performances on both day and night, especially on night. In addition, TRUST on day images performs better than TRUST on night. Both results indicating that day thermal contrast helps to unmix urban areas. Thus, day information helps to improve night unmixing when using TRUST-DNS.

Finally, for the temperature performances study, we have decided to compare pixel by pixel the 8m LST obtained directly with the TES method to the aggregation (with the Wien's law) of the unmixed LSTs, also at 8m, but with intra-pixel information. This choice grounds on two main issues: 1) the spatial distribution of materials within a 8m pixel is not known and then comparing 8m unmixed LSTs to 4m LSTs from TES is not direct, and 2) comparing pixel by pixel 8m unmixed LSTs with 4m LSTs from TES for each material within the pixel leads to errors containing contributions from abundance and temperature retrieval errors. So, this choice allows to dissociate temperature retrieval errors from abundance ones.

Relationship between LST and materials

Analysing the sign of the correlation coefficient between the abundance of a given endmember and the TES 8m LST allows to characterize the impact of this endmember on the urban LST: negative correlations indicate that the endmember mainly cools the area, while on the other hand positive correlations indicate that the endmember mainly heats the area.

Then, this study allows to link urban elements such as: roofs with red bricks, roofs with concrete or roofs with asphalt, with high daytime temperatures and low nighttime ones, showing the low thermal inertia of these materials, see figures 8 and 12 for daytime analysis and figures 9 and 13 for nighttime analysis. Thus, the correlation coefficient between the TRUST-DNS material abundance and the TES 8m LST for these materials during daytime is respectively : $R = 0.76$, $R = 0.29$ and $R = 0.42$, while during nighttime it is: $R = -0.43$ $R = -0.68$ $R = -0.47$. On the other hand natural elements such as: water, vegetation and other roads (mainly bare soil) tend to cool the area, in particular during the day (see figures 8 and 12), with negative daytime and nighttime correlations coefficients of $R = -0.91$, $R = -0.78$ and $R = -0.35$ during daytime and $R = -0.28$, $R = -0.35$ and $R = -0.18$ during nighttime. The endmember appearing as contributing to an increase of urban LSTs both during daytime and nighttime is "Roads of Asphalt" with $R = 0.33$ during daytime (see figures 8 and 12) and $R = 0.39$ during nighttime (see figures 9 and 13).

6. Conclusions

In this article, TRUST unmixing method has been applied on DESIREX 2008 daytime and nighttime images of Madrid city center. In addition, a new version of TRUST, called TRUST-DNS for Day and Night Synergy, has been developed to take advantage of available day and night images. Thus, from initial 4m radiance images, 8m ones have been generated by aggregation. This allows to use the DESIREX 2008 classification map at 4m resolution as a reference for the abundance retrieval study. Even if endmembers selection has been based on the existing DESIREX classification, the definition of their mean temperature and emissivity spectra was done by visually choosing 5 pixels (at 8 m resolution) per material and by applying TES algorithm on these pixels. This endmembers characterization can be applied on any image without needing previous information and it was also the one chosen in Cubero-Castan et al. 2014 [15]. It has been shown that both TRUST and TRUST-DNS can be applied on 8-band airborne images of urban environments at 8m resolution. Thus, these methods provide subpixel material abundances and temperatures which are in agreement respectively with the DESIREX classification and the TES temperature retrieval algorithm directly applied on 8m radiance images. In addition, it has been shown that TRUST-DNS better delineates urban objects such as streets or buildings and that their unmixed

temperatures outperform those from TRUST. This can be understood since day and night synergies are exploited. Hence, this paper shows the applicability of TRUST and TRUST-DNS on a challenging study case (highly heterogeneous image at 8m resolution with 8 thermal bands), compared to those previously studied on Cubero-Castan works [9,10,15].

The use of an airborne campaign with higher resolution images should be envisaged in order to discriminate the main source of errors in the abundance retrieval performances among: 1) non accurate classification not considering mixed pixels at 4m or 2) TRUST inaccuracies. Having higher than 4m resolution initial images will allow to increase the accuracy of the classification and to increase the ratio between the undersampled unmixed images and the reference. Thus, the analysis of the TRUST performances should be more precise. In addition, the main perspective of this work is the improvement of TRUST-DNS to be applied on urban environments at degraded resolutions (tens of meters). Cubero-Castan et al. 2015 [10] showed that the TRUST performances strongly decrease when 3 pure materials are considered in a pixel. Then, in these highly heterogeneus environments, where several pure materials (more than two) are found in pixels with sizes between 100 and 1000 m^2, TRUST is expected to provide lower performances. Nevertheless, coupling day and night images may provide supplementary constraints helping to unmix with a higher number of endmembers allowed in each pixel.

Author Contributions: Conceptualization, C.G.-B., A.M. and X.B.; methodology, C.G.-B., A.M. and X.B.; software, C.G.-B. and A.M.; validation, C.G.-B. and A.M; formal analysis, C.G.-B., A.M., V.A. and X.B.; investigation, C.G.-B., A.M., V.A. and X.B.; writing—original draft preparation, C.G.-B.; writing—review and editing, C.G.-B., A.M., V.A. and X.B.; funding acquisition, X.B.

Funding: This research was funded by C.N.E.S in the A.P.R CATUT framework. The data has been collected under E.S.A contract number 21717/08/I-LG. The APC was funded by ONERA-DOTA.

Acknowledgments: The authors wish to thank Jose A. Sobrino for providing the DESIREX 2008 campaign data and for stimulating discussions. The authors want also to thank C.N.E.S and ONERA for funding this research and APC.

Conflicts of Interest: The authors declare no conflict of interest.

1. Core Writing Team, R.P.; (eds.), L.M. Climate Change 2014: Synthesis Report. Contribution of Working Groups I, II and III to the Fifth Assessment Report of the Intergovernmental Panel on Climate Change. Technical report, IPCC, Geneva, Switzerland, 2014.
2. Zhou, D.; Xiao, J.; Bonafoni, S.; Berger, C.; K, D.; Zhou, Y.; Frolking, S.; Yao, R.; Qiao, Z.; Sobrino, J. Satellite remote sensing of surface urban heat islands: progress, challenges and perspectives. *Remote Sensing* **2019**.
3. Robine, J.M.; Cheung, S.; Roy, S.L.; Oyen, H.V.; Griffiths, C.; Michel, J.P.; Herrmann, F. Death toll exceeded 70000 in Europe during the summer 2003. *Comptes Rendus Biologies* **2008**.
4. Tiangco, M.; Lagmay, A.; Argete, J. ASTER-based study of the night-time urban heat island effect in Metro Manila. *International Journal of Remote Sensing* **2008**, *29*, 2799–818.
5. Anniballe, R.; Bonafoni, S.; Pichierri, M. Spatial and temporal trends of the surface and air heat island over Milan using MODIS data. *Remote Sensing of Environment* **2014**, *150*, 163–171.
6. Jin, M.; Dickinson, R. Land surface skin temperature climatology: benefitting from the strengths of satellite observations. *Environmental Research Letters* **2010**, *5*, 044004.
7. Sobrino, J.; Bianchi, R.; Paganini, M.; Sòria, G.; Jiménez-Muñoz, J.; Oltra-Carrió, R.; Mattar, C.; Romaguera, M.; Franch, B.; Hidalgo, V.; Cuenca, J.; Julien, Y.; Atitar, M.; Fernández-Renau, A.; Gómez, J.; De Miguel, E.; de la Cámara, Ó.G.; Jiménez, M.; Prado, E.; Rodríguez-Cantano, R.; Ruiz, I.; Nerry, F.; Najjar, G.; Kastendeutch, P.; Pujadas, M.; Molero, F.; Moreno, J.; Alonso, L.; Fernández, F.; Galán, E.; Cañada, R.; Romero, J.; Calpe-Maravilla, J.; Camps-Valls, G.; Bosch-Magraner, M.; Puente-Robles, R.; Cordero-Salvador, J.; Torres-Carrero, J.; Duque-Cuesta, M.; Moya, F.; Labajo, A.; Hidalgo-Rodríguez, J.; Acero, J.; Hernández-Martín, E.; Martilli, A.; Salamanca-Palou, F.; Gimeno-Presa, L.; Pigeon, G. DESIREX 2008: Dual-use European Security IR Experiment 2008. Technical report, European Space Agency, 2009.

8. Deng, C.; Wu, C. Estimating very high resolution urban surface temperature using a spectral unmixing and thermal mixing approach. *International Journal of Applied Earth Observation and Geoinformation* **2013**, *23*, 155–164.
9. Cubero-Castan, M.; Briottet, X.; an V. Achard, M.S.; Chanussot, J. Physic based aggregation model for the unmixing of temperature and optical properties in the infrared domain. Proceedings of the 4th Workshop on Hyperspectral Image and Signal Processing (WHISPERS); , 2012.
10. Cubero-Castan, M.; Chanussot, J.; Achard, V.; Briottet, X.; Shimoni, M. A physics-based unmixing method to estimate subpixel temperatures on mixed pixels. *IEEE Transactions on Geoscience and Remote Sensing* **2015**, *53*, 1894–1904.
11. Heinz, D.C.; Chang, C.I. Fully constrained least squares linear spectral mixture analysis method for material quantification in hyperspectral imagery. *IEEE Transactions on Geoscience and Remote Sensing* **2001**, *39*, 529–545.
12. Naughton, J.; McDonald, W. Evaluating the variability of urban land surface temperatures using drone observations. *Remote Sensing* **2019**, *11*, 1722.
13. Collins, E.F.; Roberts, D.A.; Borel, C.C. Spectral mixture analysis of simulated thermal infrared spectrometry data: an initial temperature estimated bounded TESSMA search approach. *IEEE Transactions on Geoscience and Remote Sensing* **2001**, *39*, 1435–1446.
14. Li, Z.L.; Tang, B.H.; Wu, H.; Ren, H.; Yan, G.; Wan, Z.; Trigo, I.F.; Sobrino, J.A. Satellite-derived land surface temperature: current status and perspectives. *Remote Sensing of Environment* **2013**, *131*, 14–37.
15. Cubero-Castan, M. Étude du démélange en imagerie hyperspectrale infrarouge. PhD thesis, Université de Grenoble, 2014.
16. Sobrino, J.; Bianchi, R.; Paganini, M.; Sòria, G.; Oltra-Carrió, R.; Romaguera, M.; Jiménez-Muñoz, J.; Cuenca, J.; Hidalgo, V.; Franch, B.; Mattar, C.; Julien, Y.; Moreno, J.; Alonso, L.; Fernández-Renau, A.; Gómez, J.; De Miguel, E.; Gutiérrez, Ó.; Jiménez, M.; Prado, E.; Rodríguez-Cantano, R.; Ruiz, I.; Nerry, F.; Najjar, G.; Kastendeutch, P.; Pujadas, M.; Molero, F.; Martilli, A.; Salamanca-Palou, F.; Fernández, F.; Galán, E.; Cañada, R.; Hernández, E.; Hidalgo, J.; Acero, J.; Romero, J.; Moya, F.; Gimeno, L. Urban heat island and urban thermography project DESIREX 2008. 33rd International Symposium on Remote Sensing of Environment, ISRSE, 2009.
17. Sobrino, J.; Oltra-Carrió, R.; Sòria-Barres, G.; Jiménez-Muñoz, J.C.; Franch, B.; Hidalgo, V.; Mattar, C.; Julien, Y.; Cuenca, J.; Romaguera, M.; Gómez, J.A.; Miguel, E.D.; Bianchi, R.; Paganini, M. Evaluation of the surface urban heat island effect in the city of Madrid by thermal remote sensing. *International Journal of Remote Sensing* **2013**, *34*.
18. Sobrino, J.A.; Oltra-Carrio, R.; Jimenez-Muñoz, J.C.; Julien, Y.; Soria, G.; Franch, B.; Mattar, C. Emissivity mapping over urban areas using a classification-based approach: Application to the Dual-use Eropean Security IR Experiment (DESIREX). *International Journal of Applied Earth Observation and Geoinformation* **2012**, *18*, 141–147.
19. Oltra-Carrió, R. Thermal remote sensing of urban areas. The case study of the Urban Heat Island of Madrid. PhD thesis, Universitat de Valencia, 2013.
20. Gillespie, A.; Rokugawa, S.; Matsunaga, T.; Cothern, J.S.; Hook, S.; Kahle, A.B. A temperature and emissivity separation algortihm for Advanced Spaceborn Thermal Emission and Reflection radiometer (ASTER) images. *IEEE Transactions on Geoscience and Remote Sensing* **1998**, *36*, 1113–1126.
21. Kay, S.M. *Fundamentals of statistical signal processing: estimation theory*; Englewood Cliffs, 1993.